ISTITUTO NAZIONALE FISICA NUCLEARE

INFN/AE -86/5
2 aprile 1986

L. Rolandi

SPACE RESOLUTION OF THE TPC

Servizio Riproduzione della
Sezione di Trieste dell'INFN

SPACE RESOLUTION OF THE T.P.C.

Luigi Rolandi
Dipartimento di Fisica and Sezione I.N.F.N.
Trieste, Italy

Talk given at the XIV International Winter Meeting on
Fundamental Physics,
Sant Feliu de Giuxols, Catalonia, Spain
March 17-22 1986

ABSTRACT

The principle of coordinate measurement of the Time Projection Chamber is discussed together with the various factors that influence the measuring accuracy in the sagitta direction. Some experimental results on the spatial resolution with different cathode geometry are presented and are compared with the theory.

The TPC is a large solid angle tracking device which can provide a good spatial resolution by giving for each space point on a track a simultaneous and unambiguous measurement of the three space coordinates r, r-Φ and z. It has an excellent pattern recognition capabilities even in high particle density environment.

Fig. 1 shows a schematic view of a TPC. The chamber sits in an uniform magnetic field parallel to the drift electric field. The ionization electrons from a charged particle passing through the chamber drift parallel to the axis of the chamber. The electrons are detected when they reach the endcaps by proportional wires stretched across the end planes where their amplitude, position and time of arrival are measured.

The magnetic field bends the particles at right angles to the cylinder radius vector and the particle momentum is determined by a precise measurement of the sagitta of the particle helix projected onto the end plane. The magnetic field has also another purpose: it reduces the transverse diffusion of the electrons during their drift, giving an increased precision to the r-Φ measurement that is the most important because is the one that influences the momentum resolution. This is the foundamental idea of the TPC.

The principle of coordinate measurement is shown in Fig. 2. The ionization electrons move in the gas under the influence of the electric and the magnetic field and reach the anode wires. For each track segment the two coordinates in the end plane are given by cathode pads which trasmit the electric pulses from the avalance at the sense wires into amplifiers connected to each pad. The pads are arranged such that the induced signal is spread over few of them and the precision in r-Φ is obtained interpolating between them. The z coordinate is found from the drift time and the known drift velocity.

The r-Φ resolution depends on several factors. Some of them are connected to the transport of the electrons in the drift volume. Some others influence directly the avalance localization along the wire. The errors are then treated accordingly to their physical origin in two categories:

- Displacement of the drift trajectories due to field inhomogeneities
- Statistical variation of the electron swarm due to the finite number of electron and their clustering

In addition one has to consider other errors from mechanical and electronic surces (as misalignement of the pads or noise into the preamplifiers) that will be not discussed in detail. Their overall contribution can be kept of the order of 100 μm by a suitable electronic design and carefull machining of the endplates.

DISPLACEMENT OF THE DRIFT TRAJECTORIES

In the case of inhomogeneous $\vec{E}$ and $\vec{B}$ field, the drift velocity vector *)

$$v = [\mu E/(i+w^2\tau^2)]\ [\hat{E}+w\tau[\hat{E}x\hat{B}]+w^2\tau^2(\hat{E}\cdot\hat{B})\hat{B}] \qquad (1)$$

depends on the two gas constants μ and wτ; μ is the mobility and wτ is the dimensionless product of the electron cyclotron frequency w=(e/m)B and the mean free time τ between collisions of the electrons with the gas molecules. From this equation, where E is the magnitude of the electric field and $\hat{E}$ and $\hat{B}$ are unit vectors, one deduces that field inhomogeneities will create distorsions of the drift trajectories. Knowing the fields these distorsions can be corrected with the help of (1).

---

*) This formula is a suitable approximation of the drift velocity field, for a complete formulation see ref. [1].

Fig. 3 shows the dependence of the direction of the drift velocity on $\omega\tau$. The influence of the electric field is strongest for $\omega\tau << 1$, since the electrons travel maily along the electric field lines, whereas they follow mainly the magnetic field lines for $\omega\tau >> 1$. For $\omega\tau = 1$ the $(\vec{E}x\vec{B})$ component is maximal.

Fig. 4 from reference [2] shows the dependence of $\omega\tau$ on the electric field for some mixtures of Argon with hidrocarbons. We see that at some value of the drift field and for low concentration on methane in argon at atmospheric pressure it is possible to obtain $\omega\tau$ values up to 15 in a magnetic field of 2 T.

The distorsion in the azimuthal direction, which influences the measurement of the sagitta, is induced by the azimuthal components of the fields and also by their radials components due to the $\vec{E}x\vec{B}$ term of (1). There are advantages at large $\omega\tau$: the effects of the radial components are reduced by the factor $1/\omega\tau$ and those of the azimuthal component of the electric field by a factor $1/(\omega\tau)^2$. The suppression of the effects correlated to the electric field is very important because whilst the magnetic field can be measured and is stable, this may be not the case for the electric field. It could be distorted by uncontrollable and local charge accumulations [3].

Given the expected value of $\omega\tau$ the distorsions in the direction of the sagitta can be largely reduced but, in spite of the precautions that one can put in the design of the magnetic field, one cannot exclude distortion of few 100 μm when the electrons have to drift over distances of the order of 1 meter. This is just a bit larger of what could be ignored.

A laser calibration system can be used to monitor these distortions and to calculate the corrections of the real

tracks. For this calibration purpose only the straightness of the laser beams is important, neither their position nor their brightness needs to be known with precision.

The feasibility of this calibration system has been tested [4] in a magnetic field up to 1.2 T. Laser ionization tracks 0.6 m long were drifted over 1.3 m, and their displacement was mesured as a function of the magnetic field strength. Figures 5 and 6 show that when the current is reversed in the magnet the antisymmetric displacements of a laser track (Δ) are proportional to $w\tau/(1+w^2\tau^2)$, and the symmetric track displacements (S) are proportional to $w^2\tau^2/(1+w^2\tau^2)$, as contained in (1). Assuming an homogeneous electric field it is possible to calculate with this equation the integral over z of the radial component of the magnetic field from the measured displacements. Figure 7 (from Ref. [4]) shows the perfect agreement of this calculation with the measured map of the magnetic field.

The results of the tests described above have shown that with this procedure it is possible to compute and to correct the track distorsions induced by the inhomogeneities of the fields, so that the accuracy of the track reconstruction is solely limited by ionization statistics, mechanical and electrical imperfections.

STATISTICAL VARIATION OF THE AVALANCHE POSITION

The accuracy of the measurement of the electron swarm centre of gravity is affected by the following three effects, which are caused by the discontinuous nature of the ionization process.

a) The diffusion process over a drift distance L displaces each electron by a mean square value of 2DL/v. The diffusion constant D depends on the magnetic field approximately like

$$D(B) = D(O)/(1+w^2\tau^2) \qquad (2)$$

Here lines another advantage of a high value of $w\tau$.

The electron cloud measured over one pad row consists of N_e electrons. Their centre position measured at right angles to the track has a variance of

$$2LD(B)/(vN_e) \qquad (3)$$

b) The angular wire effect arises when the track makes an angle α with the normal to the wire in the end plane (Fig. 8a). The ionization charge is then collected on the sense wire, not in one point but over a distance $d \cdot \tan\alpha$. The position of the centre of gravity of the charge has a variance of $(1/N_{eff})(d^2/12) \cdot \tan^2\alpha$, where N_{eff} represents the effective number of fluctuating charges collected over the wire gap d; N_{eff} may be smaller than the number of primary clusters created in d because of the cluster size variation, or it may approach the total number of electrons if, owing to strong diffusion, the electrons have loss the space correlation of their primary clustering.

The presence of the magnetic field makes this effect asymmetric and, on an average, larger: the electrons, as they are collected in the cylindrical field of the sense wire, travel across the magnetic field lines, and the $(\hat{E}x\hat{B})$ term in (1) gives them a velocity component along the wire. The average angle under which they approach the wire is denoted by ψ (see Fig. 8b). Now the ionization charge is smeared out over a distance $d(\tan\alpha - \tan\psi)$, and the variance of the centre position along the wire is

$$(d^2/12\ N_{eff})(\tan\alpha - \tan\psi)^2 \qquad (4)$$

This influence of the magnetic field was discovered at TRIUMF [5]; in Fig.9 we see the resolution measured there as a function of the angle α. It was large and asymmetric.

When more than one wire contributes to the signal

induced in a pad row, there is a statistical gain which is represented by a corresponding increase of N_{eff}.

c) The angular pad effect arises when the track makes an angle β with the normal to the pad row in the end plane. The ionization charge is spread out over a distance h tan β along the pad row, h being the length of a pad. Therefore, the position of the centre of the charges has a variance of

$$(h^2/12\ N_{eff})\ \tan^2\beta\ . \qquad (5)$$

Here, the effective number N_{eff} of fluctuating charges has the same meaning as above; it refers to the gas sample thickness h. We have omitted statistical factors from the β-dependence of the gas thickness. Comparing (5) and (4) we notice that the angular pad effect is relatively large because h is several times as large as d. Also, when h increases, the pad effect goes up and the wire effect goes down. With the approximation that N_{eff} is proportional to h, (4) is proportional to 1/h, and (5) is proportional to h.

The greater part of the angular pad effect can be corrected [3,6] when use is made of the measured pulse height of the wires. In practice it has been possible to correct a fraction $f_{corr} = 0.95$ of (5) in clean cases.

EXPERIMENTAL RESULTS

Collecting all the statistical contributions from above we may parametrize the rΦ resolution for the case where the track makes an angle α with the wire normal and the pad rows follow the wires (Berkeley geometry, $\alpha = \beta$):

$$\sigma^2 = \sigma_0^2+\sigma_d^2 L/\cos\alpha+\sigma_1^2(\tan\alpha-\tan\psi)^2\cos\alpha+\sigma_2^2\tan^2\alpha\cos\alpha \qquad (6)$$

where L is the drift length in metres. (Here we have included the statistical cosα factors describing the variation of the gas sample thickness, and the diffusion

term contains the projection factor (1/cosα) applicable to the diffusion of an inclined line of electrons).

In a test chamber which reproduced the Berkeley geometry, the resolution was measured in an argon-methane mixture (90:10) at 1.5 T and a drift length of 3 cm, as a function of the angle α [6]. Curve A in Fig. 10 shows the result. After applying the angular pad correction we obtained curve B. A fit of (6) yielded

$$\sigma_0 = (155 \pm 25)\ \mu m$$
$$\sigma_1 = (340 \pm 30)\ \mu m$$
$$\psi = (29 \pm 3)^\circ$$
$$\sigma_2 = (1000 \pm 50)\ \mu m \text{ before correction}$$
$$\sigma_2 = (230 \pm 80)\ \mu m \text{ after correction}$$

An independent measurement tells us that under these conditions

$$\sigma_d \simeq 80\ \mu m\ .$$

These numbers implied that in this geometry it was essential to do the angular pad correction, and that the two angular effects were then comparable in size.

A NEW GEOMETRY

Although the importance of the angular pad term in the resolution can be drastically reduced using the pulse heights of the wires, this is not really satisfying since these corrections can only be applied if the wire signals of the track are clean and not overlapped in time the signals of other tracks. With the expected large track densities in jets at LEP energies this might be only rarely the case. Moreover, the experimental values of σ_1 and σ_2 (correction applied) show that in the case of the Berkeley geometry only a minor improvement of the resolution could still be

obtained by increasing the pad length, because of the two competing angular effects.

A big step forward was made in 1983 with the proposal of new geometry for the end plate of the ALEPH TPC [7], based on circular rings of radial pads (Fig. 11). With this geometry the angular pad effect disappears for the high momentum tracks coming from the interaction point, which, having radial trajectories, are always at $\beta = 0$ (Fig. 12). This then made it possible to increase the length of the pads to 30 mm, reducing the contributions of the angular wire effect and of the diffusion to the resolution. Collecting more charge also increased the ratio signal/electronic noise.

Figure 13 from ref. [8] shows the computed momentum resolution of the Aleph detector as function of the momentum of the tracks with the new endplate geometry. The angular wire effect is reduced by a factor 0.66 when the pad length is changed from 8 to 30 mm.

EXPERIMENTAL EVIDENCE OF THE ADVANTAGES OF THE NEW GEOMETRY

A measurement of the spatial resolution obtainable with long pads has been done recently with a small TPC equipped with four pad rows [9]. The orientation of the sense wires could be changed with respect to the pads to simulate the local geometry of the ALEPH TPC. The chamber was operated with an argon-methane mixture of 90:10 in a magnetic field of 1.5 T. Particles of momentum larger than 15 GeV parallel to the pad axis ($\beta \simeq 0$) were measured.

The space resolution can be parametrized (with $\beta = 0$) as follows:

$$\sigma^2 = \sigma_0^2 + \sigma_d^2/L + \sigma_1^2 \cos^2\alpha(\tan\alpha - \tan\psi)^2 \qquad (7)$$

The measured resolution σ is shown in curve C of Fig. 10 as

a function of the angle α. A fit of (7) to these data gives

$$\sigma_0 = (104 \pm 1)\ \mu m$$
$$\sigma_1 = (219 \pm 3)\ \mu m$$
$$\psi = (32 \pm 0.5)^\circ .$$

This measurement of ψ is in perfect agreement with the one mentioned earlier, and the ratio of the two results for σ_1 being 0.64 ± 0.06 also agrees very well with the expected value of 0.66 [8].

Another experiment was done with this chamber in order to study the combined influence of the angular effect and the diffusion on the spatial resolution at zero magnetic field ($\psi = 0$). The idea was to determine σ ,which should not depend on the magnetic field, at a different single-electron diffusion. The average drift length was 4.5 cm, corresponding at B = 0 to a single-electron diffusion of 1.3 mm comparable to the sense wire pitch. Fitting the data with (7) gives $\sigma_1 = 125 \pm 5\ \mu m$, indicating that the diffusion indeed reduces the angular wire effect.

A single-electron diffusion of 1.3 mm at B = 1.5 T corresponds to a drift of 220 cm, which is just the maximum drift length in the ALEPH TPC. Therefore this value of σ_1, together with the measured value of ψ , can be used to predict the resolution in the ALEPH TPC for stiff tracks at maximum drift lengths. This is plotted as curve D in Fig.10.

REFERENCES

[1] W.P. Allis, in: Handbuch der Physik, vol. 23 ed. S. Flugge (Springer, Berlin, 1956).

[2] A.R. Clark et al.: Pep-4 Proposal (1976).

[3] A. Barbaro-Galtieri: Traking with the Pep-4 TPC, TPC-LBL-82-24 (1982).

[4] S.R. Amendolia et al.: Calibration of Field Inhomogeneities in a Time Projection Chamber with laser rays. Nucl. Instrum. Methods A235, 296 (1985).

[5] C.K. Hargrove et al.: The spatial resolution of the Time Projection Chamber at Triumf. Nucl. Instrum. Methods 219, 461 (1984).

[6] S.R. Amendolia et al.: ExB and angular effects in the avalance localization along the wire with cathode pad read-out. Nucl. Instrum. Methods 217, 317 (1983).

[7] J. Steinberger: Note on radially long pads and sector geometry, Aleph-TPC note 95 (1983).

[8] J. Steinberger: Ionization, pad length and TPC resolution, Aleph note 146 (1985).

[9] W. Blum et al.: Measurement of avalance broadening caused by the wire ExB effect, presented at the Vienna Wire Chamber Conference 1986.

FIGURE CAPTIONS

1 - Schematic view of a TPC.
2 - Principle of coordinate measurement.
3 - Schematic view of the drift velocity direction as function of wt.
4 - Dependence of wt on the reduced electric field for different gas mixtures.
5 - Antisymmetric displacement of the measured coordinate as function of the magnetic field.
6 - Symmetric displacement of the measured coordinate as function of the magnetic field.
7 - Measured distorsions (points) induced by the magnetic field compared to those calculated using the field map (curves).
8 - Spread of charges along the wire.
9 - Resolution as function of the crossing angle α.
10 - Resolution as function of the angle α at B = 1.5 T.
Curve A: Berkeley geometry, no angular corrections;
curve B: Berkeley geometry, with angular corrections;
curve C: 30 mm radial pads, 4 cm drift;
curve D: 30 mm radial pads, 220 cm drift.
11 - End plate of the Aleph TPC.
12 - Definition of the angles.
13 - Momentum resolution as function of momentum for charged particles in the Aleph detector.

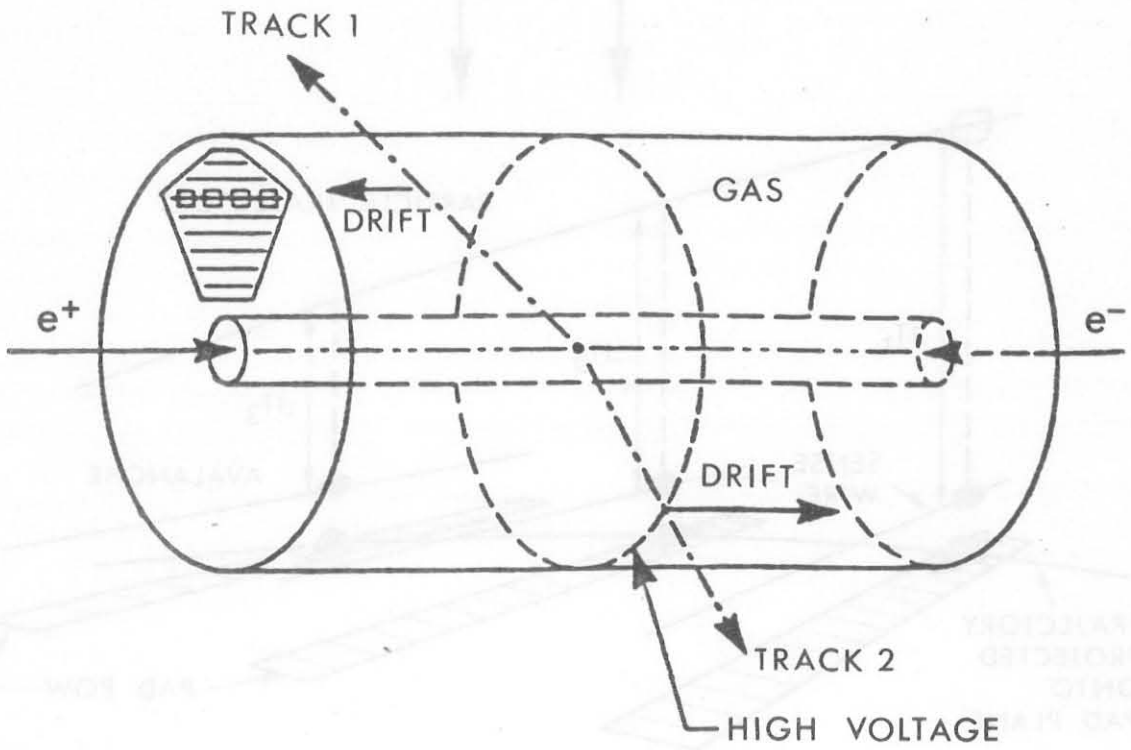

FIG. 1

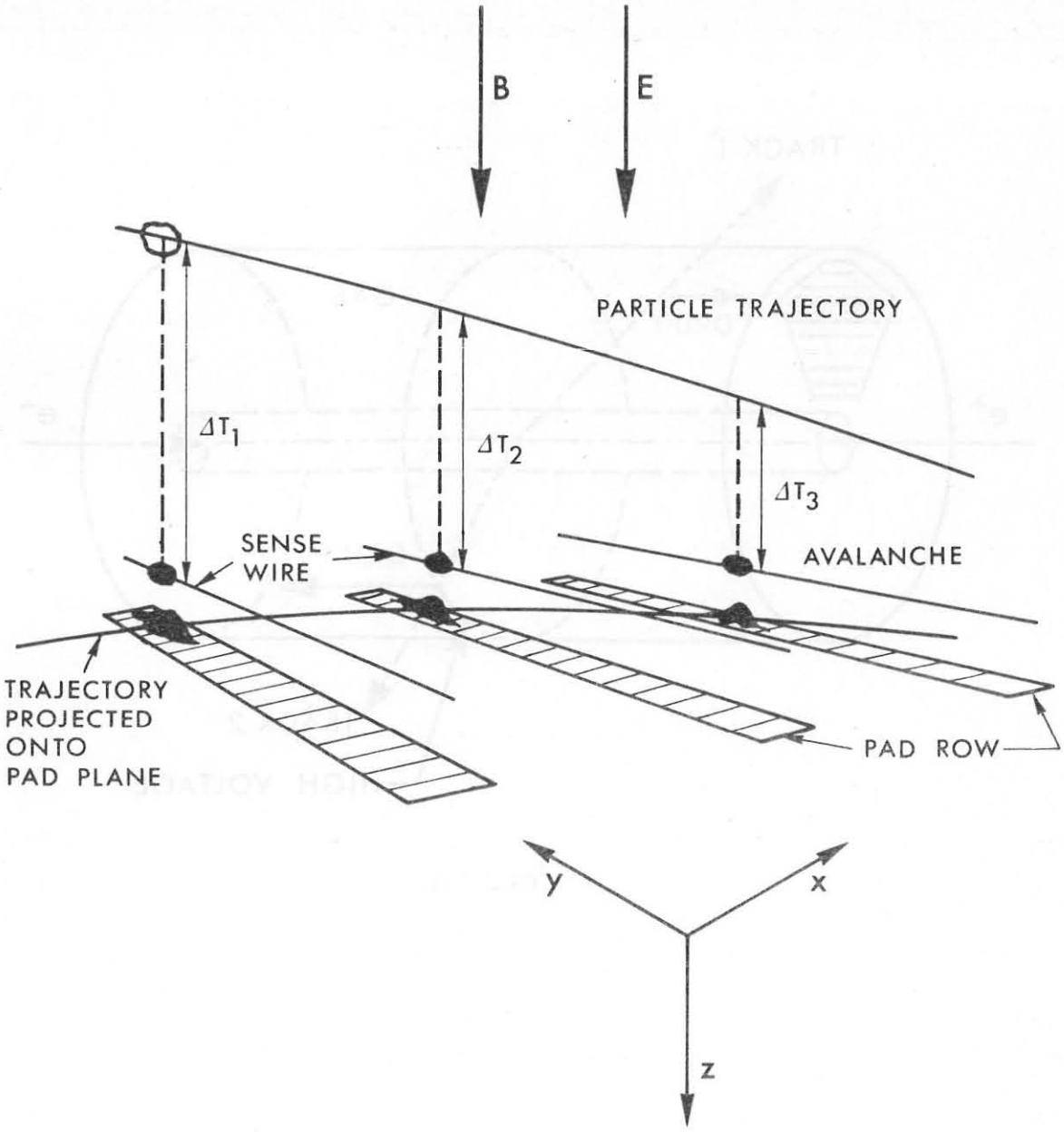
B
E
PARTICLE TRAJECTORY
ΔT_1
ΔT_2
ΔT_3
SENSE WIRE
AVALANCHE
TRAJECTORY PROJECTED ONTO PAD PLANE
PAD ROW
y
x
z

FIG. 2

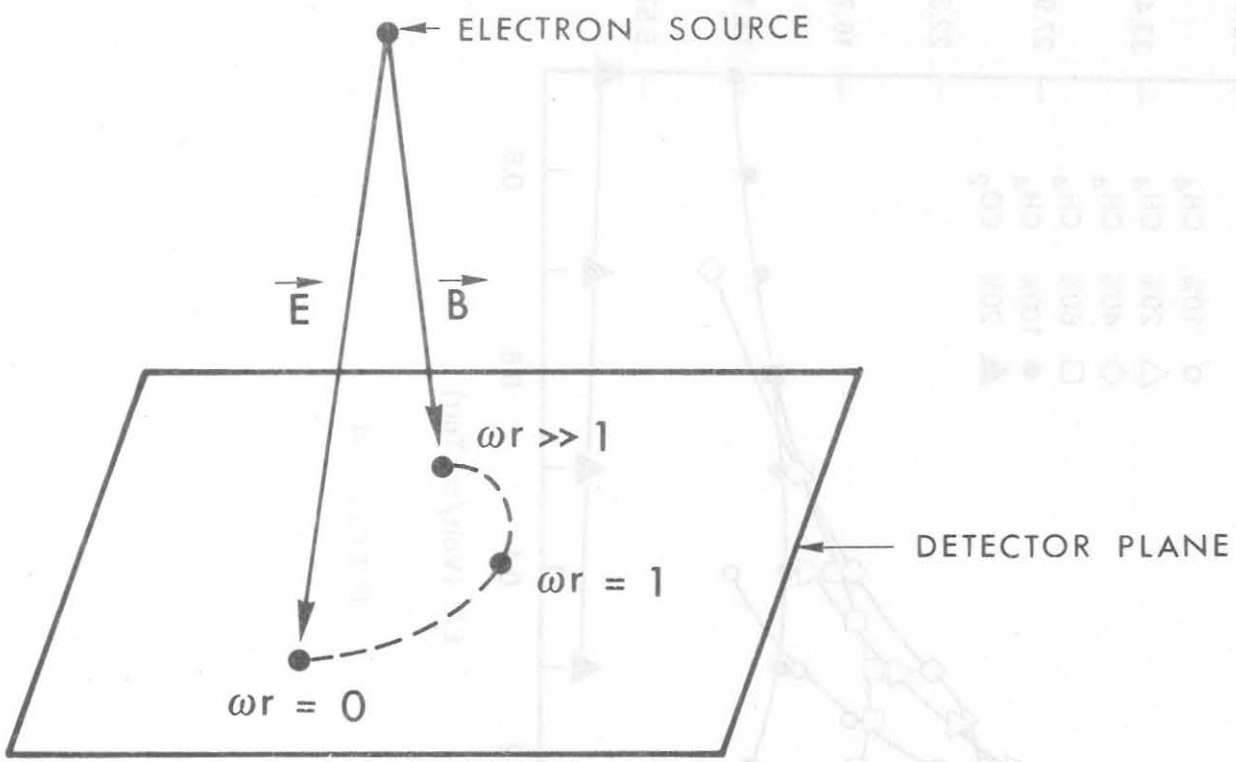

FIG. 3

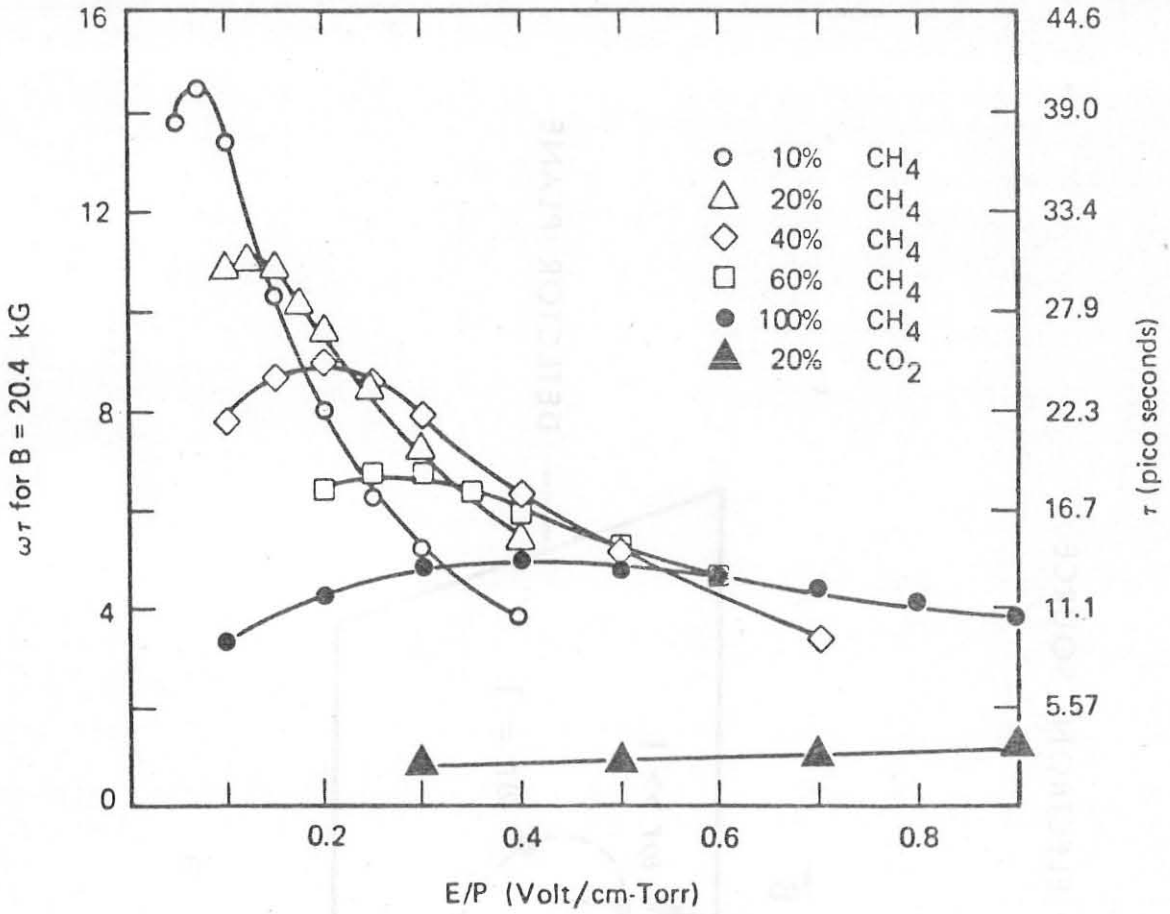
16
12
8
4
0
44.6
39.0
33.4
27.9
22.3
16.7
11.1
5.57
0.2
0.4
0.6
0.8
E/P (Volt/cm-Torr)
ωτ for B = 20.4 kG
τ (pico seconds)
10% CH4
20% CH4
40% CH4
60% CH4
100% CH4
20% CO2

FIG. 4

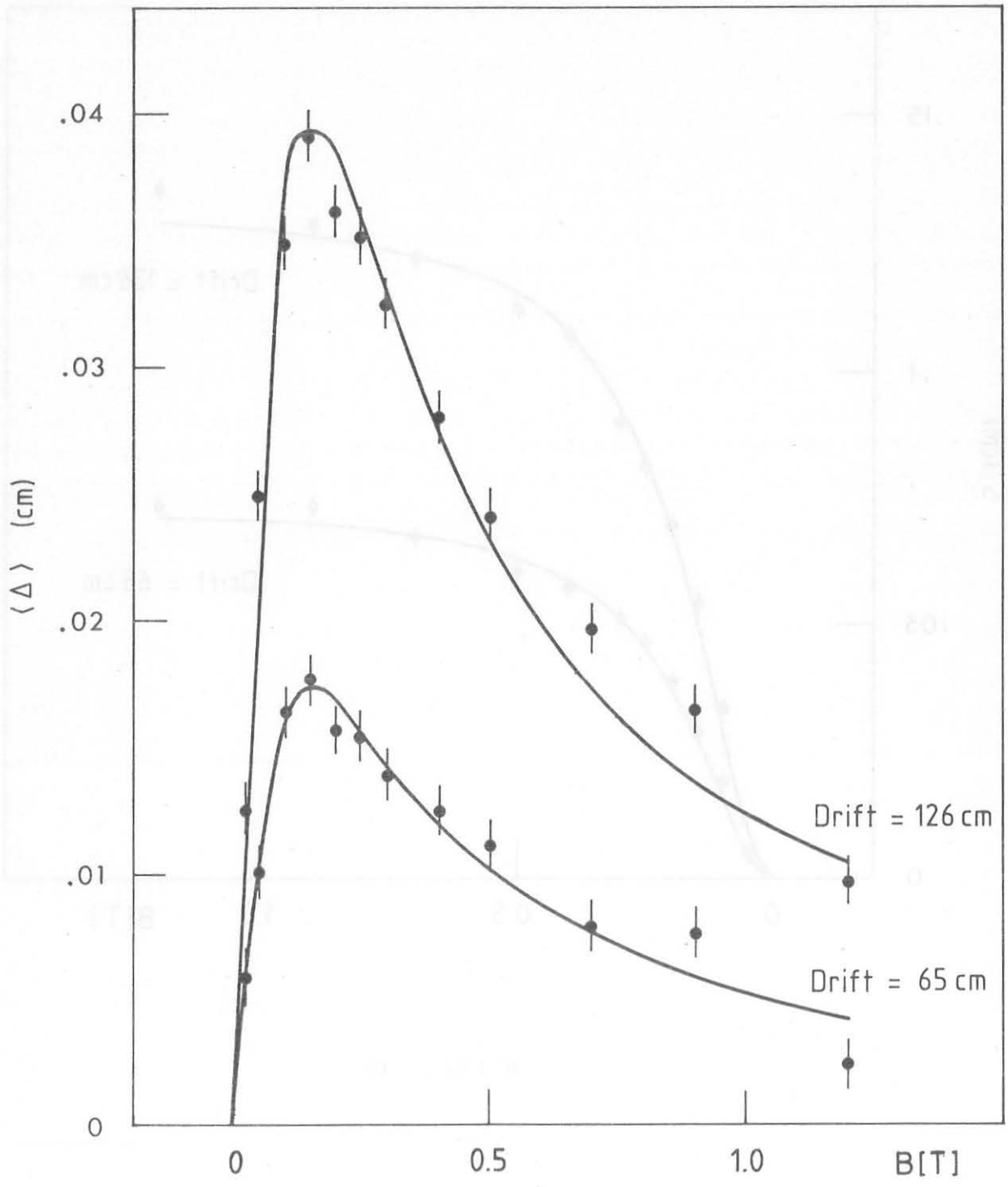

FIG. 5

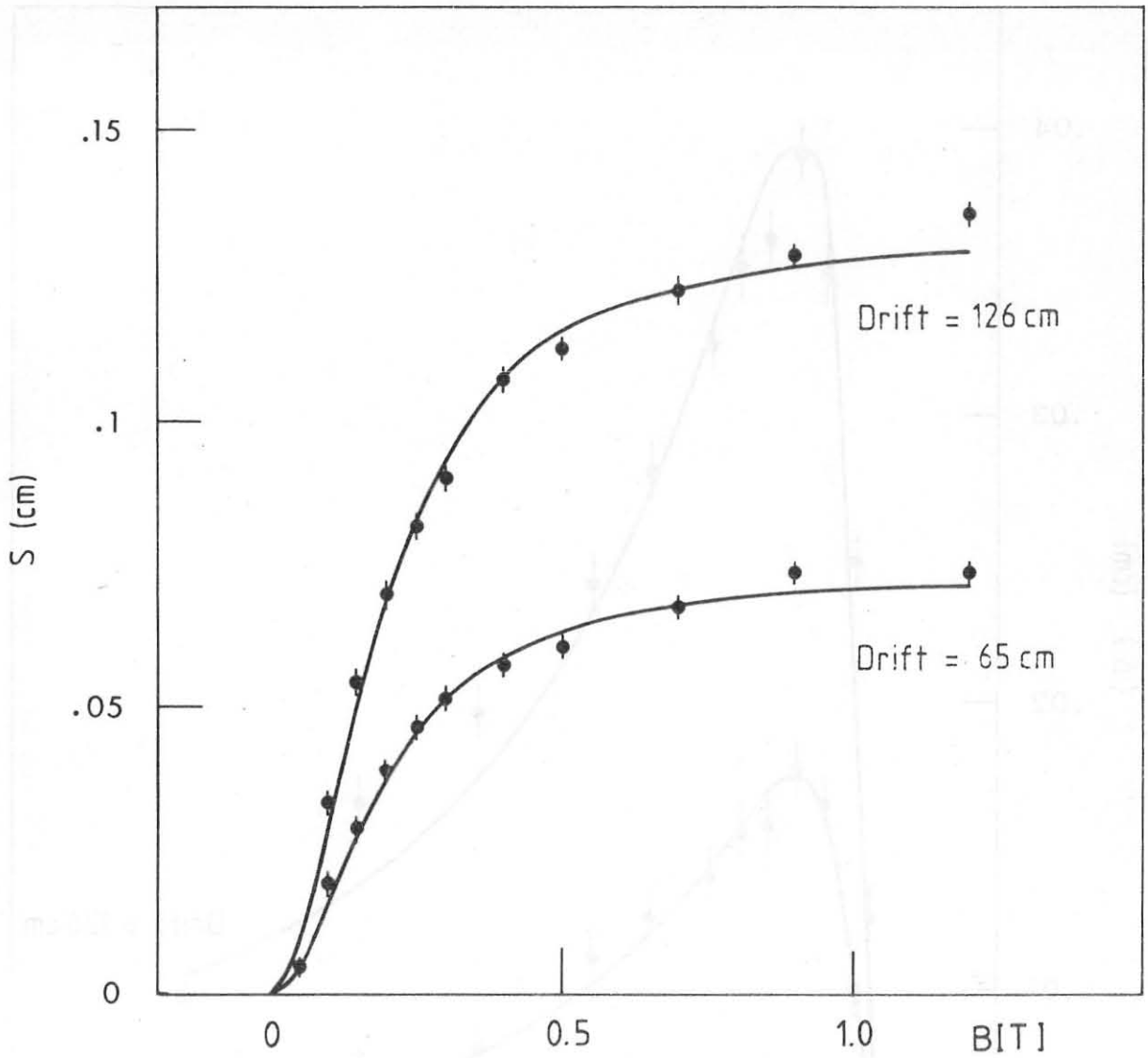

FIG. 6

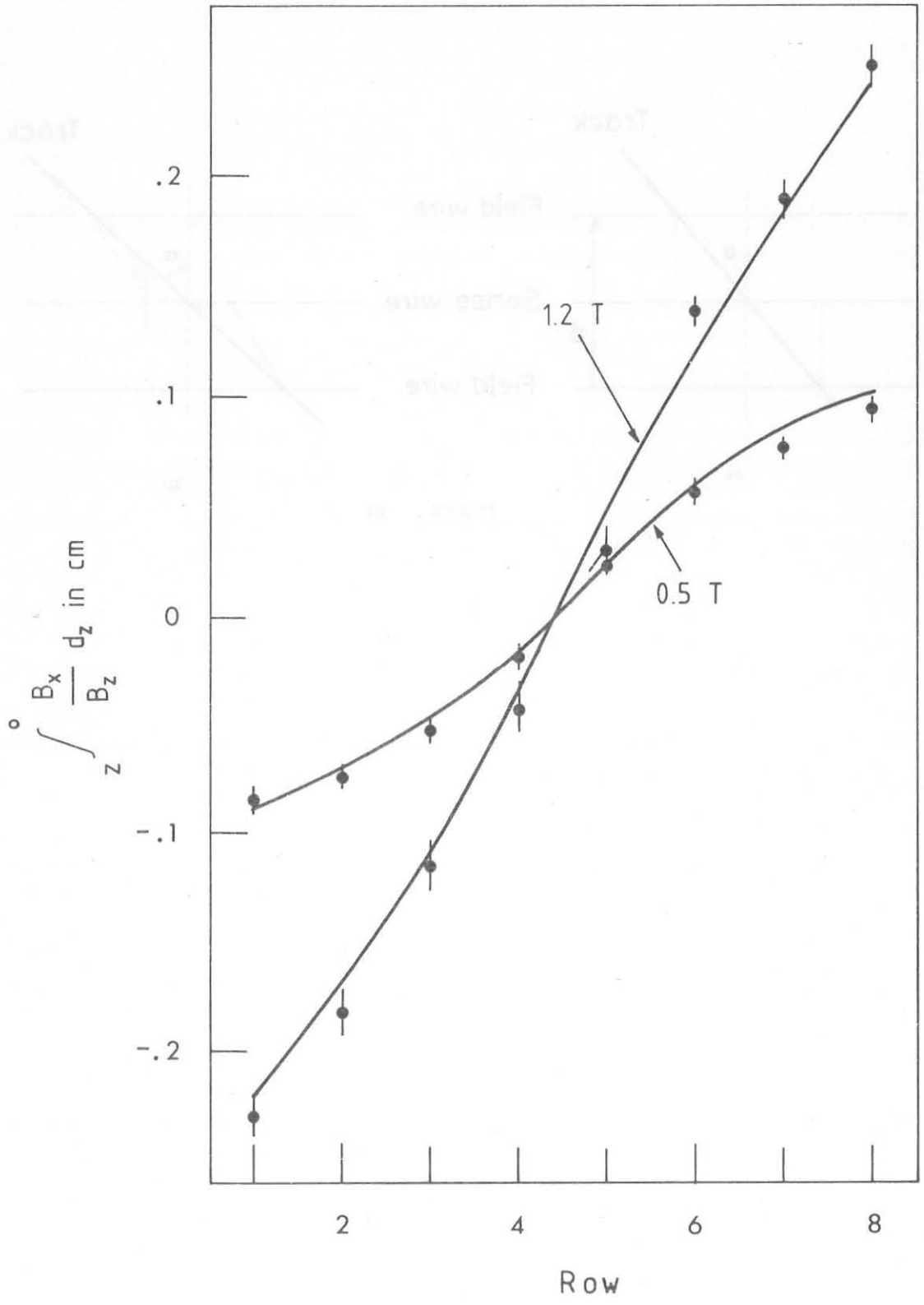

FIG. 7

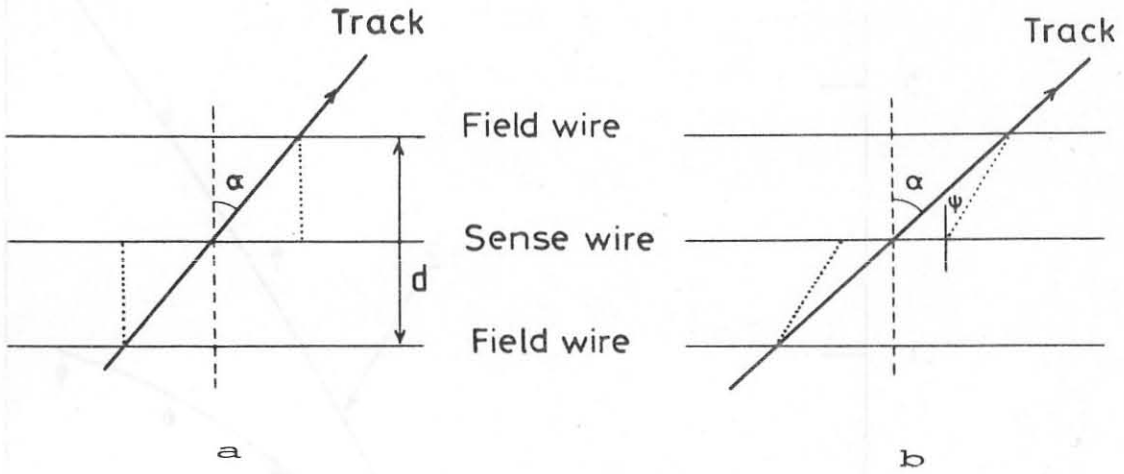

FIG. 8

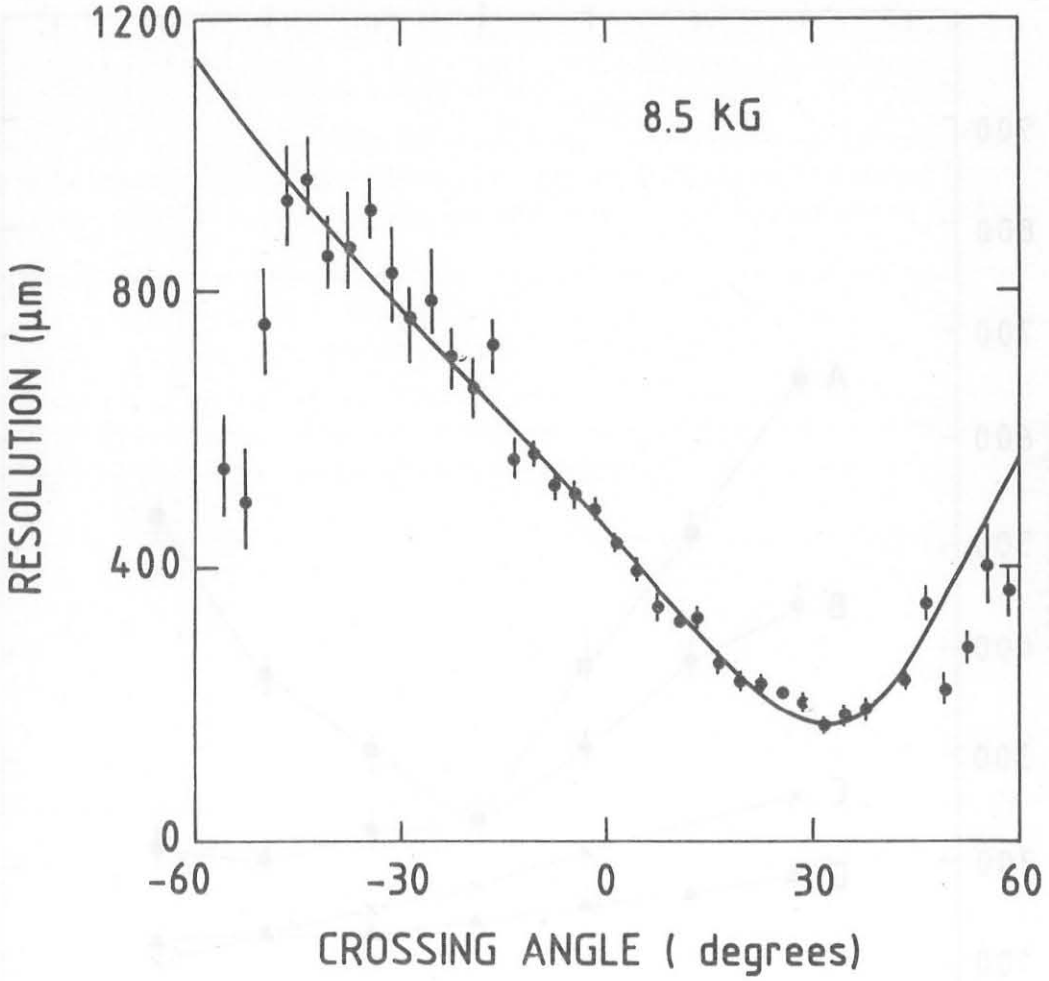
1200
800
400
0
8.5 KG
RESOLUTION (μm)
-60
-30
0
30
60
CROSSING ANGLE (degrees)

FIG. 9

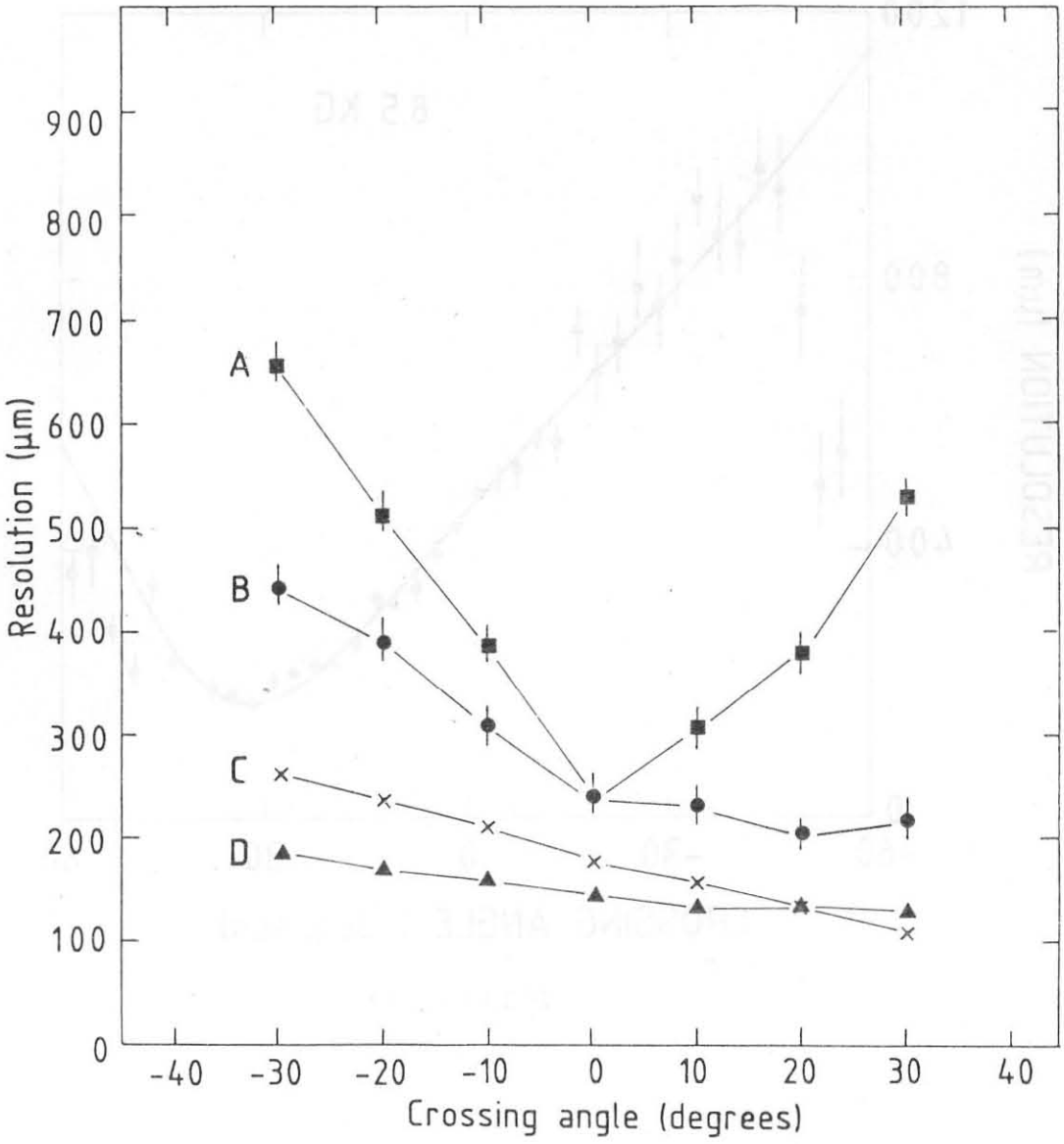
900
800
700
600
500
400
300
200
100
0
Resolution (μm)
A
B
C
D
-40
-30
-20
-10
0
10
20
30
40
Crossing angle (degrees)

FIG. 10

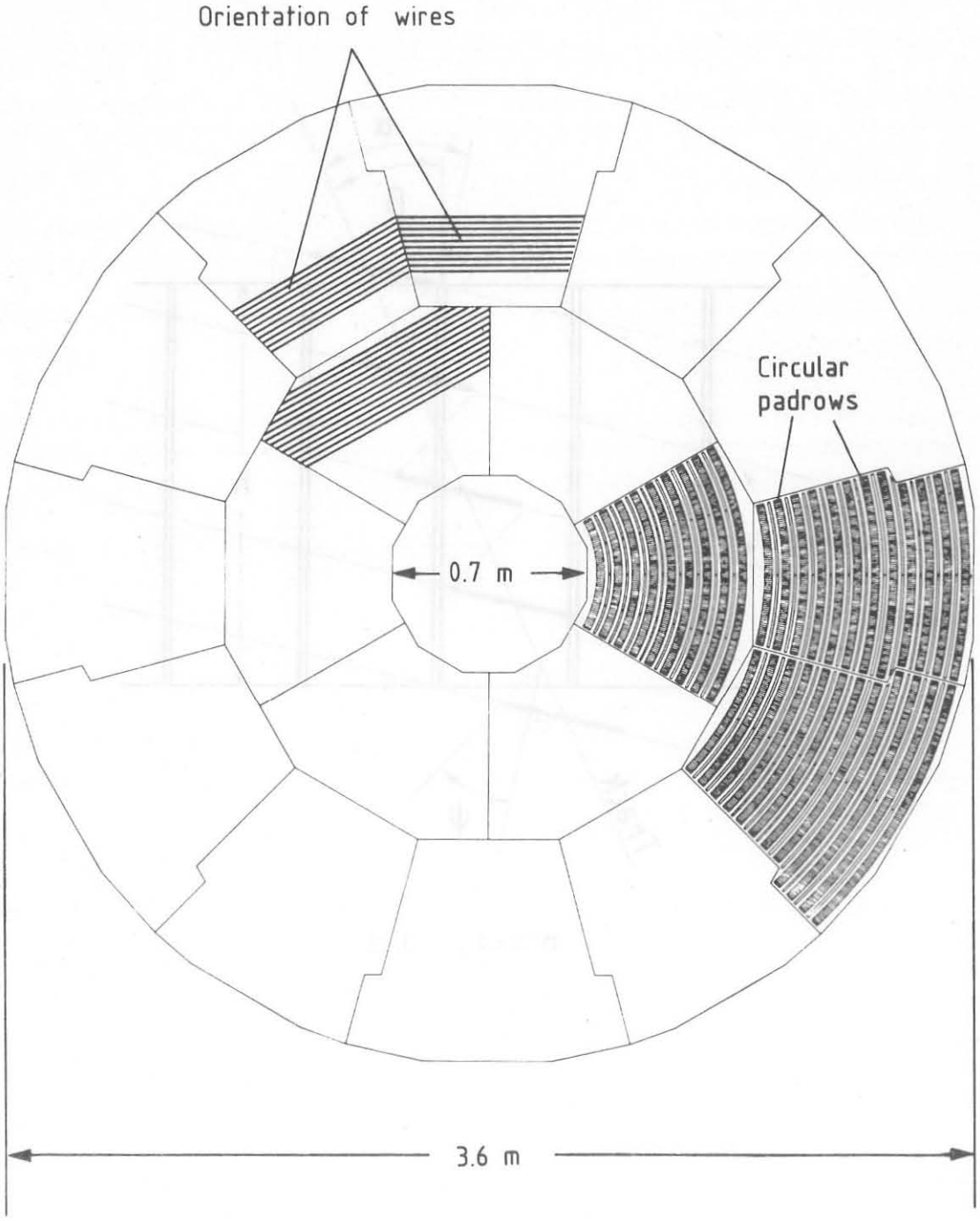

FIG. 11

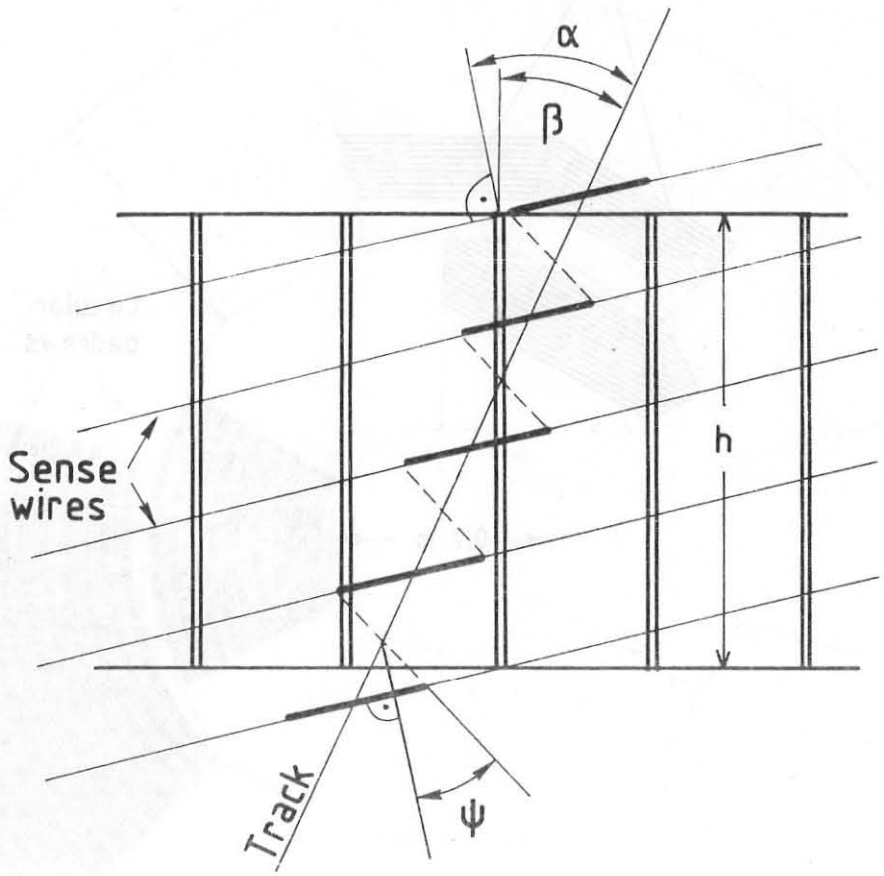

FIG. 12

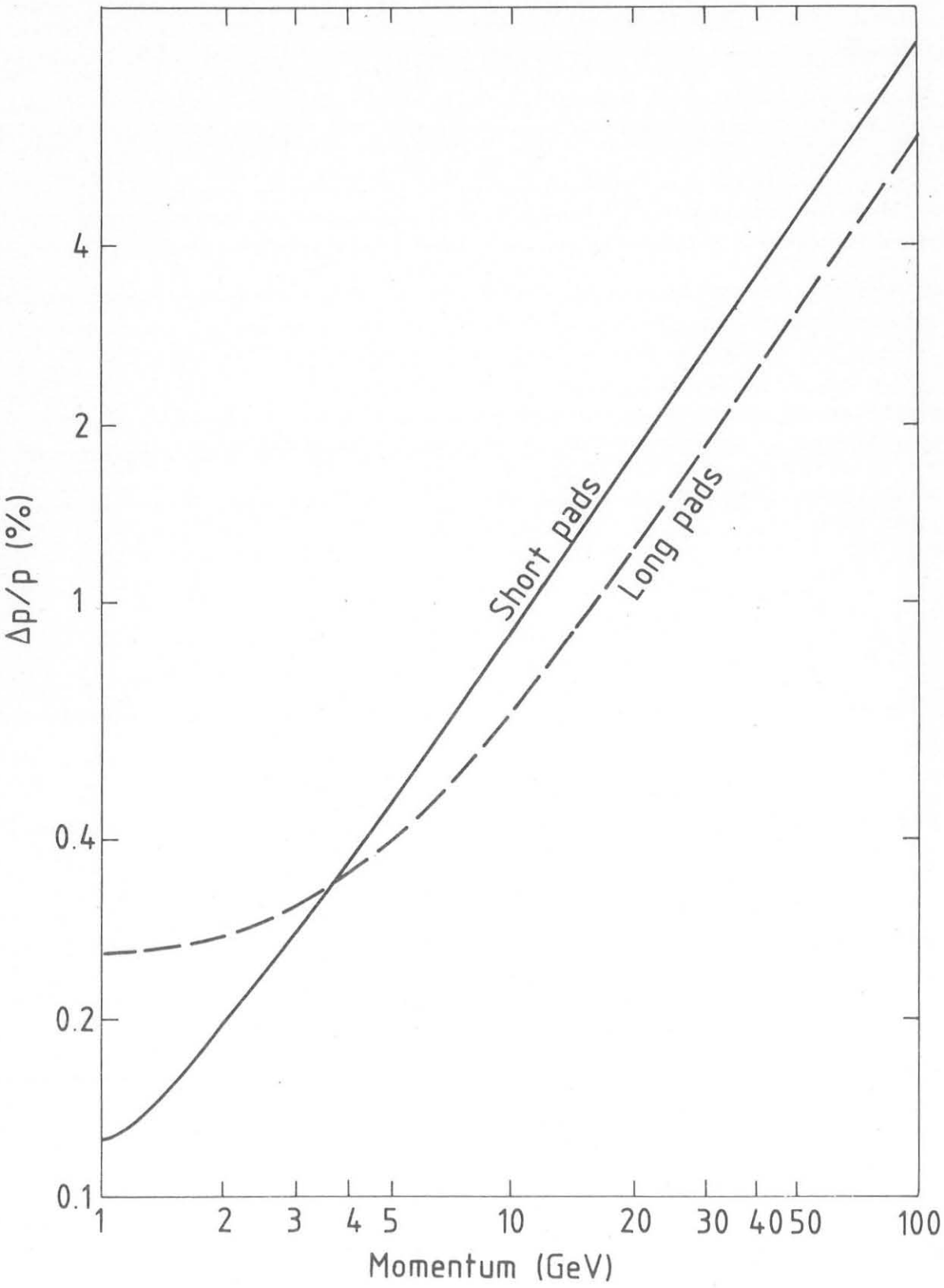
Δp/p (%)
4
2
1
0.4
0.2
0.1
Short pads
Long pads
1
2
3
4
5
10
20
30
40
50
100
Momentum (GeV)

FIG. 13